FERMILAB-PUB-22-441-AD-PPD-SCD-TD
(Accepted)

Draft version May 31, 2022
Typeset using LATEX **twocolumn** style in AASTeX63

A search for photons with energies above 2 10^{17} eV using hybrid data from the low-energy extensions of the Pierre Auger Observatory

P. Abreu,[1] M. Aglietta,[2,3] J.M. Albury,[4] I. Allekotte,[5] K. Almeida Cheminant,[6] A. Almela,[7,8]
J. Alvarez-Muñiz,[9] R. Alves Batista,[10] J. Ammerman Yebra,[9] G.A. Anastasi,[2,3] L. Anchordoqui,[11] B. Andrada,[7]
S. Andringa,[1] C. Aramo,[12] P.R. Araújo Ferreira,[13] E. Arnone,[14,3] J. C. Arteaga Velázquez,[15] H. Asorey,[7]
P. Assis,[1] G. Avila,[16] E. Avocone,[17,18] A.M. Badescu,[19] A. Bakalova,[20] A. Balaceanu,[21] F. Barbato,[18,22]
J.A. Bellido,[4,23] C. Berat,[24] M.E. Bertaina,[14,3] G. Bhatta,[6] P.L. Biermann,[25] V. Binet,[26] K. Bismark,[27,7]
T. Bister,[13] J. Biteau,[28] J. Blazek,[20] C. Bleve,[24] J. Blümer,[29] M. Boháčová,[20] D. Boncioli,[17,22] C. Bonifazi,[30,31]
L. Bonneau Arbeletche,[32] N. Borodai,[6] A.M. Botti,[7] J. Brack,[33] T. Bretz,[13] P.G. Brichetto Orchera,[7]
F.L. Briechle,[13] P. Buchholz,[34] A. Bueno,[35] S. Buitink,[36] M. Buscemi,[37] M. Büsken,[27,7] K.S. Caballero-Mora,[38]
L. Caccianiga,[39,40] F. Canfora,[10,41] I. Caracas,[42] R. Caruso,[43,37] A. Castellina,[2,3] F. Catalani,[44] G. Cataldi,[45]
L. Cazon,[9] M. Cerda,[46] J.A. Chinellato,[32] J. Chudoba,[20] L. Chytka,[47] R.W. Clay,[4] A.C. Cobos Cerutti,[48]
R. Colalillo,[49,12] A. Coleman,[50] M.R. Coluccia,[45] R. Conceição,[1] A. Condorelli,[18,22] G. Consolati,[40,51]
F. Contreras,[16] F. Convenga,[29] D. Correia dos Santos,[52] C.E. Covault,[53] S. Dasso,[54,55] K. Daumiller,[29]
B.R. Dawson,[4] J.A. Day,[4] R.M. de Almeida,[52] J. de Jesús,[7,29] S.J. de Jong,[10,41] J.R.T. de Mello Neto,[31,56]
I. De Mitri,[18,22] J. de Oliveira,[57] D. de Oliveira Franco,[32] F. de Palma,[58,45] V. de Souza,[59] E. De Vito,[58,45]
A. Del Popolo,[43,37] M. del Río,[16] O. Deligny,[60] L. Deval,[29,7] A. di Matteo,[3] M. Dobre,[21] C. Dobrigkeit,[32]
J.C. D'Olivo,[61] L.M. Domingues Mendes,[1] R.C. dos Anjos,[62] M.T. Dova,[63] J. Ebr,[20] R. Engel,[27,29] I. Epicoco,[58,45]
M. Erdmann,[13] C.O. Escobar,[64] A. Etchegoyen,[7,8] H. Falcke,[10,65,41] J. Farmer,[66] G. Farrar,[67] A.C. Fauth,[32]
N. Fazzini,[64] F. Feldbusch,[68] F. Fenu,[14,3] B. Fick,[69] J.M. Figueira,[7] A. Filipčič,[70,71] T. Fitoussi,[29] T. Fodran,[10]
T. Fujii,[72,66] A. Fuster,[7,8] C. Galea,[10] C. Galelli,[39,40] B. García,[48] A.L. Garcia Vegas,[13] H. Gemmeke,[68]
F. Gesualdi,[7,29] A. Gherghel-Lascu,[21] P.L. Ghia,[60] U. Giaccari,[10] M. Giammarchi,[40] J. Glombitza,[13] F. Gobbi,[46]
F. Gollan,[7] G. Golup,[5] M. Gómez Berisso,[5] P.F. Gómez Vitale,[16] J.P. Gongora,[16] J.M. González,[5]
N. González,[73] I. Goos,[5,29] D. Góra,[6] A. Gorgi,[2,3] M. Gottowik,[42] T.D. Grubb,[4] F. Guarino,[49,12] G.P. Guedes,[74]
E. Guido,[3,14] S. Hahn,[29,7] P. Hamal,[20] M.R. Hampel,[7] P. Hansen,[63] D. Harari,[5] V.M. Harvey,[4] A. Haungs,[29]
T. Hebbeker,[13] D. Heck,[29] G.C. Hill,[4] C. Hojvat,[64] J.R. Hörandel,[10,41] P. Horvath,[47] M. Hrabovský,[47]
T. Huege,[29,36] A. Insolia,[43,37] P.G. Isar,[75] P. Janecek,[20] J.A. Johnsen,[76] J. Jurysek,[20] A. Kääpä,[42]
K.H. Kampert,[42] B. Keilhauer,[29] A. Khakurdikar,[10] V.V. Kizakke Covilakam,[7,29] H.O. Klages,[29] M. Kleifges,[68]
J. Kleinfeller,[46] F. Knapp,[27] N. Kunka,[68] B.L. Lago,[77] N. Langner,[13] M.A. Leigui de Oliveira,[78] V. Lenok,[29]
A. Letessier-Selvon,[79] I. Lhenry-Yvon,[60] D. Lo Presti,[43,37] L. Lopes,[1] R. López,[80] L. Lu,[81] Q. Luce,[27]
J.P. Lundquist,[71] A. Machado Payeras,[32] G. Mancarella,[58,45] D. Mandat,[20] B.C. Manning,[4] J. Manshanden,[82]
P. Mantsch,[64] S. Marafico,[60] F.M. Mariani,[39,40] A.G. Mariazzi,[63] I.C. Mariş,[73] G. Marsella,[83,37]
D. Martello,[58,45] S. Martinelli,[29,7] O. Martínez Bravo,[80] M. Mastrodicasa,[17,22] H.J. Mathes,[29] J. Matthews,[84]
G. Matthiae,[85,86] E. Mayotte,[76,42] S. Mayotte,[76] P.O. Mazur,[64] G. Medina-Tanco,[61] D. Melo,[7] A. Menshikov,[68]
S. Michal,[47] M.I. Micheletti,[26] L. Miramonti,[39,40] S. Mollerach,[5] F. Montanet,[24] L. Morejon,[42] C. Morello,[2,3]
M. Mostafá,[87] A.L. Müller,[20] M.A. Muller,[32] K. Mulrey,[10,41] R. Mussa,[3] M. Muzio,[67] W.M. Namasaka,[42]
A. Nasr-Esfahani,[42] L. Nellen,[61] G. Nicora,[88] M. Niculescu-Oglinzanu,[21] M. Niechciol,[34] D. Nitz,[69]
I. Norwood,[69] D. Nosek,[89] V. Novotny,[89] L. Nožka,[47] A Nucita,[58,45] L.A. Núñez,[90] C. Oliveira,[59] M. Palatka,[20]
J. Pallotta,[88] P. Papenbreer,[42] G. Parente,[9] A. Parra,[80] J. Pawlowsky,[42] M. Pech,[20] J. Pękala,[6] R. Pelayo,[91]
J. Peña-Rodriguez,[90] E.E. Pereira Martins,[27,7] J. Perez Armand,[92] C. Pérez Bertolli,[7,29] L. Perrone,[58,45]
S. Petrera,[18,22] C. Petrucci,[17,22] T. Pierog,[29] M. Pimenta,[1] V. Pirronello,[43,37] M. Platino,[7] B. Pont,[10]
M. Pothast,[41,10] P. Privitera,[66] M. Prouza,[20] A. Puyleart,[69] S. Querchfeld,[42] J. Rautenberg,[42] D. Ravignani,[7]
M. Reininghaus,[29,7] J. Ridky,[20] F. Riehn,[1] M. Risse,[34] V. Rizi,[17,22] W. Rodrigues de Carvalho,[10]
J. Rodriguez Rojo,[16] M.J. Roncoroni,[7] S. Rossoni,[82] M. Roth,[29] E. Roulet,[5] A.C. Rovero,[54] P. Ruehl,[34]
A. Saftoiu,[21] M. Saharan,[10] F. Salamida,[17,22] H. Salazar,[80] G. Salina,[86] J.D. Sanabria Gomez,[90] F. Sánchez,[7]
E.M. Santos,[92] E. Santos,[20] F. Sarazin,[76] R. Sarmento,[1] C. Sarmiento-Cano,[7] R. Sato,[16] P. Savina,[81]
C.M. Schäfer,[29] V. Scherini,[58,45] H. Schieler,[29] M. Schimassek,[27,7] M. Schimp,[42] F. Schlüter,[29,7] D. Schmidt,[27]
O. Scholten,[36] H. Schoorlemmer,[10,41] P. Schovánek,[20] F.G. Schröder,[50,29] J. Schulte,[13] T. Schulz,[29]
S.J. Sciutto,[63] M. Scornavacche,[7,29] A. Segreto,[93,37] S. Sehgal,[42] R.C. Shellard,[94] G. Sigl,[82] G. Silli,[7,29]
O. Sima,[95,21] R. Smau,[21] R. Šmída,[66] P. Sommers,[87] J.F. Soriano,[11] R. Squartini,[46] M. Stadelmaier,[29,7] D. Stanca,[21]
S. Stanič,[71] J. Stasielak,[6] P. Stassi,[24] A. Streich,[27,7] M. Suárez-Durán,[73] T. Sudholz,[4] T. Suomijärvi,[28]
A.D. Supanitsky,[7] Z. Szadkowski,[96] A. Tapia,[97] C. Taricco,[14,3] C. Timmermans,[41,10] O. Tkachenko,[29] P. Tobiska,[20]
C.J. Todero Peixoto,[44] B. Tomé,[1] Z. Torrès,[24] A. Travaini,[46] P. Travnicek,[20] C. Trimarelli,[17,22] M. Tueros,[63]

spokespersons@auger.org

This document was prepared by Pierre Auger Collaboration using the resources of the Fermi National Accelerator Laboratory (Fermilab), a U.S. Department of Energy, Office of Science, HEP User Facility. Fermilab is managed by Fermi Research Alliance, LLC (FRA), acting under Contract No. DE-AC02-07CH11359.

R. Ulrich,[29] M. Unger,[29] L. Vaclavek,[47] M. Vacula,[47] J.F. Valdés Galicia,[61] L. Valore,[49,12] E. Varela,[80] A. Vásquez-Ramírez,[90] D. Veberič,[29] C. Ventura,[56] I.D. Vergara Quispe,[63] V. Verzi,[86] J. Vicha,[20] J. Vink,[98] S. Vorobiov,[71] H. Wahlberg,[63] C. Watanabe,[31] A.A. Watson,[99] A. Weindl,[29] L. Wiencke,[76] H. Wilczyński,[6] D. Wittkowski,[42] B. Wundheiler,[7] A. Yushkov,[20] O. Zapparrata,[73] E. Zas,[9] D. Zavrtanik,[71,70] M. Zavrtanik,[70,71] L. Zehrer,[71]

The Pierre Auger Collaboration

Laboratório de Instrumentação e Física Experimental de Partículas – LIP and Instituto Superior Técnico – IST, Universidade de Lisboa – UL, Lisboa, Portugal

Osservatorio Astrofisico di Torino (INAF), Torino, Italy

INFN, Sezione di Torino, Torino, Italy

University of Adelaide, Adelaide, S.A., Australia

Centro Atómico Bariloche and Instituto Balseiro (CNEA-UNCuyo-CONICET), San Carlos de Bariloche, Argentina

Institute of Nuclear Physics PAN, Krakow, Poland

Instituto de Tecnologías en Detección y Astropartículas (CNEA, CONICET, UNSAM), Buenos Aires, Argentina

Universidad Tecnológica Nacional – Facultad Regional Buenos Aires, Buenos Aires, Argentina

Instituto Galego de Física de Altas Enerxías (IGFAE), Universidade de Santiago de Compostela, Santiago de Compostela, Spain

IMAPP, Radboud University Nijmegen, Nijmegen, The Netherlands

Department of Physics and Astronomy, Lehman College, City University of New York, Bronx, NY, USA

INFN, Sezione di Napoli, Napoli, Italy

RWTH Aachen University, III. Physikalisches Institut A, Aachen, Germany

Università Torino, Dipartimento di Fisica, Torino, Italy

Universidad Michoacana de San Nicolás de Hidalgo, Morelia, Michoacán, México

Observatorio Pierre Auger and Comisión Nacional de Energía Atómica, Malargüe, Argentina

Università dell'Aquila, Dipartimento di Scienze Fisiche e Chimiche, L'Aquila, Italy

Gran Sasso Science Institute, L'Aquila, Italy

University Politehnica of Bucharest, Bucharest, Romania

Institute of Physics of the Czech Academy of Sciences, Prague, Czech Republic

"Horia Hulubei" National Institute for Physics and Nuclear Engineering, Bucharest-Magurele, Romania

INFN Laboratori Nazionali del Gran Sasso, Assergi (L'Aquila), Italy

Universidad Nacional de San Agustin de Arequipa, Facultad de Ciencias Naturales y Formales, Arequipa, Peru

Univ. Grenoble Alpes, CNRS, Grenoble Institute of Engineering Univ. Grenoble Alpes, LPSC-IN2P3, 38000 Grenoble, France

Max-Planck-Institut für Radioastronomie, Bonn, Germany

Instituto de Física de Rosario (IFIR) – CONICET/U.N.R. and Facultad de Ciencias Bioquímicas y Farmacéuticas U.N.R., Rosario, Argentina

Karlsruhe Institute of Technology (KIT), Institute for Experimental Particle Physics, Karlsruhe, Germany

Université Paris-Saclay, CNRS/IN2P3, IJCLab, Orsay, France

Karlsruhe Institute of Technology (KIT), Institute for Astroparticle Physics, Karlsruhe, Germany

International Center of Advanced Studies and Instituto de Ciencias Físicas, ECyT-UNSAM and CONICET, Campus Miguelete – San Martín, Buenos Aires, Argentina

Universidade Federal do Rio de Janeiro, Instituto de Física, Rio de Janeiro, RJ, Brazil

Universidade Estadual de Campinas, IFGW, Campinas, SP, Brazil

Colorado State University, Fort Collins, CO, USA

Universität Siegen, Department Physik – Experimentelle Teilchenphysik, Siegen, Germany

Universidad de Granada and C.A.F.P.E., Granada, Spain

Vrije Universiteit Brussels, Brussels, Belgium

INFN, Sezione di Catania, Catania, Italy

Universidad Autónoma de Chiapas, Tuxtla Gutiérrez, Chiapas, México

Università di Milano, Dipartimento di Fisica, Milano, Italy

INFN, Sezione di Milano, Milano, Italy

Nationaal Instituut voor Kernfysica en Hoge Energie Fysica (NIKHEF), Science Park, Amsterdam, The Netherlands

Bergische Universität Wuppertal, Department of Physics, Wuppertal, Germany

Università di Catania, Dipartimento di Fisica e Astronomia "Ettore Majorana", Catania, Italy

Universidade de São Paulo, Escola de Engenharia de Lorena, Lorena, SP, Brazil

INFN, Sezione di Lecce, Lecce, Italy

Observatorio Pierre Auger, Malargüe, Argentina

Palacky University, RCPTM, Olomouc, Czech Republic
Instituto de Tecnologías en Detección y Astropartículas (CNEA, CONICET, UNSAM), and Universidad Tecnológica Nacional – Facultad Regional Mendoza (CONICET/CNEA), Mendoza, Argentina
Università di Napoli "Federico II", Dipartimento di Fisica "Ettore Pancini", Napoli, Italy
University of Delaware, Department of Physics and Astronomy, Bartol Research Institute, Newark, DE, USA
Politecnico di Milano, Dipartimento di Scienze e Tecnologie Aerospaziali , Milano, Italy
Universidade Federal Fluminense, EEIMVR, Volta Redonda, RJ, Brazil
Case Western Reserve University, Cleveland, OH, USA
Instituto de Astronomía y Física del Espacio (IAFE, CONICET-UBA), Buenos Aires, Argentina
Departamento de Física and Departamento de Ciencias de la Atmósfera y los Océanos, FCEyN, Universidad de Buenos Aires and CONICET, Buenos Aires, Argentina
Universidade Federal do Rio de Janeiro (UFRJ), Observatório do Valongo, Rio de Janeiro, RJ, Brazil
Instituto Federal de Educação, Ciência e Tecnologia do Rio de Janeiro (IFRJ), Brazil
Università del Salento, Dipartimento di Matematica e Fisica "E. De Giorgi", Lecce, Italy
Universidade de São Paulo, Instituto de Física de São Carlos, São Carlos, SP, Brazil
CNRS/IN2P3, IJCLab, Université Paris-Saclay, Orsay, France
Universidad Nacional Autónoma de México, México, D.F., México
Universidade Federal do Paraná, Setor Palotina, Palotina, Brazil
IFLP, Universidad Nacional de La Plata and CONICET, La Plata, Argentina
Fermi National Accelerator Laboratory, Fermilab, Batavia, IL, USA
Stichting Astronomisch Onderzoek in Nederland (ASTRON), Dwingeloo, The Netherlands
University of Chicago, Enrico Fermi Institute, Chicago, IL, USA
New York University, New York, NY, USA
Karlsruhe Institute of Technology (KIT), Institut für Prozessdatenverarbeitung und Elektronik, Karlsruhe, Germany
Michigan Technological University, Houghton, MI, USA
Experimental Particle Physics Department, J. Stefan Institute, Ljubljana, Slovenia
Center for Astrophysics and Cosmology (CAC), University of Nova Gorica, Nova Gorica, Slovenia
now at Hakubi Center for Advanced Research and Graduate School of Science, Kyoto University, Kyoto, Japan
Université Libre de Bruxelles (ULB), Brussels, Belgium
Universidade Estadual de Feira de Santana, Feira de Santana, Brazil
Institute of Space Science, Bucharest-Magurele, Romania
Colorado School of Mines, Golden, CO, USA
Centro Federal de Educação Tecnológica Celso Suckow da Fonseca, Nova Friburgo, Brazil
Universidade Federal do ABC, Santo André, SP, Brazil
Laboratoire de Physique Nucléaire et de Hautes Energies (LPNHE), Sorbonne Université, Université de Paris, CNRS-IN2P3, Paris, France
Benemérita Universidad Autónoma de Puebla, Puebla, México
University of Wisconsin-Madison, Department of Physics and WIPAC, Madison, WI, USA
Universität Hamburg, II. Institut für Theoretische Physik, Hamburg, Germany
Università di Palermo, Dipartimento di Fisica e Chimica "E. Segrè", Palermo, Italy
Louisiana State University, Baton Rouge, LA, USA
Università di Roma "Tor Vergata", Dipartimento di Fisica, Roma, Italy
INFN, Sezione di Roma "Tor Vergata", Roma, Italy
Pennsylvania State University, University Park, PA, USA
Centro de Investigaciones en Láseres y Aplicaciones, CITEDEF and CONICET, Villa Martelli, Argentina
Charles University, Faculty of Mathematics and Physics, Institute of Particle and Nuclear Physics, Prague, Czech Republic
Universidad Industrial de Santander, Bucaramanga, Colombia
Unidad Profesional Interdisciplinaria en Ingeniería y Tecnologías Avanzadas del Instituto Politécnico Nacional (UPIITA-IPN), México, D.F., México
Universidade de São Paulo, Instituto de Física, São Paulo, SP, Brazil
Istituto di Astrofisica Spaziale e Fisica Cosmica di Palermo (INAF), Palermo, Italy
Centro Brasileiro de Pesquisas Fisicas, Rio de Janeiro, RJ, Brazil
also at University of Bucharest, Physics Department, Bucharest, Romania
University of Łódź, Faculty of High-Energy Astrophysics,Łódź, Poland
Universidad de Medellín, Medellín, Colombia
Universiteit van Amsterdam, Faculty of Science, Amsterdam, The Netherlands
School of Physics and Astronomy, University of Leeds, Leeds, United Kingdom

Submitted to ApJ

ABSTRACT

Ultra-high-energy photons with energies exceeding 10^{17} eV offer a wealth of connections to different aspects of cosmic-ray astrophysics as well as to gamma-ray and neutrino astronomy. The recent observations of photons with energies in the 10^{15} eV range further motivate searches for even higher-energy photons. In this paper, we present a search for photons with energies exceeding 2×10^{17} eV using about 5.5 years of hybrid data from the low-energy extensions of the Pierre Auger Observatory. The upper limits on the integral photon flux derived here are the most stringent ones to date in the energy region between 10^{17} and 10^{18} eV.

Keywords: Particle astrophysics (96) — Ultra-high-energy cosmic radiation (1733) — Cosmic-ray showers (327) — Non-thermal radiation sources (1119) — Multivariate analysis (1913)

1. INTRODUCTION

The recent observations of photons with energies of a few 10^{14} eV from decaying neutral pions, both from a direction coincident with a giant molecular cloud (HAWC J1825-134, Albert et al. (2021)) and from the Galactic plane (Amenomori et al. 2021), provide evidence for an acceleration of cosmic rays to energies of several 10^{15} eV, and above, in the Galaxy. A dozen of sources emitting photons with energies up to 10^{15} eV have even been reported (Cao et al. 2021a), and in at least one of them (LHAASO J2108+515, also in directional coincidence with a giant molecular cloud), these photons might have a hadronic origin (Cao et al. 2021b). Observations of these photons are key in probing the mechanisms of particle acceleration, completing the multi-messenger approach aimed at understanding the non-thermal processes producing cosmic rays. The detection of even higher-energy photons would be of considerable interest in discovering extreme accelerators in the Galaxy. Also, should one detect photons of such energies clustered preferentially in the direction of the Galactic Center, then this could highlight the presence of super-heavy dark matter produced in the early Universe and decaying today (see, e.g., Berezinsky & Mikhailov (1999); Benson et al. (1999); Medina-Tanco & Watson (1999); Aloisio et al. (2006); Siffert et al. (2007); Kalashev & Kuznetsov (2016); Alcantara et al. (2019)).

Above 10^{17} eV, the absorption length for photons almost matches the scale of the Galaxy, and reaches that of the Local Group as the energy increases (Risse & Homola 2007). The observation of point-like sources of photons would be compelling evidence for the presence of ultra-high-energy accelerators within such a local horizon. Diffuse fluxes of photons are also expected from farther away from the interactions of ultra-high-energy cosmic rays (UHECRs) with the background photon fields permeating the extragalactic space (see, e.g., Gelmini et al. (2008); Kampert et al. (2011); Bobrikova et al. (2021)) or with the interstellar matter in the Galactic disk (Berat et al. 2022). Although the estimation of these cosmogenic photon fluxes suffers from several uncertainties of astrophysical origin, such as, in particular, the exact composition of UHECRs, they can be determined to range, at most, around 10^{-2} km^{-2} sr^{-1} yr^{-1} above 10^{17} eV and around $10^{-3.5}$ km^{-2} sr^{-1} yr^{-1} above 10^{18} eV. These cosmogenic fluxes are more than two orders of magnitude below the sensitivity of current instruments, thereby constituting a negligible background for detecting photons from point sources, extended structures, or exotic phenomena.

Previous searches for a diffuse flux of photons using data from KASCADE-Grande (Apel et al. 2017) and EAS-MSU (Fomin et al. 2017) have led to upper limits on photon fluxes of the order of 10 km^{-2} sr^{-1} yr^{-1} for energy thresholds between 10^{17} eV and 3×10^{17} eV, while at higher energies, at a threshold of 10^{18} eV, upper limits of the order of 10^{-2} km^{-2} sr^{-1} yr^{-1} were determined using data from the Pierre Auger Observatory (Savina & Pierre Auger Collaboration 2021). The aim of the study reported in this paper is to search for primary photons with energies above 2×10^{17} eV using data from the low-energy extensions of the Pierre Auger Observatory, which are briefly presented in Section 2. The data set used in this study is described in Section 3 together with the simulations needed to establish the selection criteria aimed at distinguishing photon-induced air showers from those initiated by hadronic cosmic rays. In Section 4, the specificities of the photon-induced showers are used to define discriminating observables, which are then combined to search for photon candidate events in the data. Results are given in Section 5 and, from the absence of a photon signal, upper limits on the integral photon flux are derived that improve the previous ones mentioned before. Finally, the astrophysical significance of these limits is discussed in Section 6.

2. THE PIERRE AUGER OBSERVATORY

The Pierre Auger Observatory (Aab et al. 2015a), located near Malargue, Argentina, o ers an unprecedented exposure for UHE photons. A key feature of the Pierre Auger Observatory is the hybrid concept, combining a Surface Detector array (SD) with a Fluorescence Detector (FD). The SD consists of 1600 water-Cherenkov detectors arranged on a triangular grid with a spacing of 1500 m, covering a total area of 3000 km^2. The SD is overlooked by 24 uorescence telescopes, located at four sites at the border of the array. The SD samples the lateral shower pro le at ground level, i.e., the distribution of particles as a function of the distance from the shower axis, with a duty cycle of 100 %, while the FD records the longitudinal shower development in the atmosphere above the SD. The FD can only be operated in clear, moonless nights, reducing the duty cycle to 15 %. Through combining measurements from both detector systems in hybrid events, a superior accuracy of the air-shower reconstruction can be achieved than with just one system. In the western part of the SD array, 50 additional SD stations have been placed between the existing SD stations, forming a sub-array with a spacing of 750 m and covering a total area of about 27 5 km^2. With this sub-array, air showers of lower primary energy (below 10^{18} eV) with a smaller footprint can be measured. To allow also for hybrid measurements in this energy range, where air showers develop above the eld of view of the standard FD telescopes, three additional High-Elevation Auger Telescopes (HEAT) have been installed at the FD site Coihueco, overlooking the 750 m SD array. The HEAT telescopes operate in the range of elevation angles from 30 to 60 , complementing the Coihueco telescopes operating in the 0 to 30 range. The combination of the data from both HEAT and Coihueco (HeCo data) enable uorescence measurements of air showers over a large range of elevation angles. A schematic depiction of the detector layout, including the 750 m array and HEAT, can be found in Fig. 1.

3. DATA SAMPLES AND SIMULATIONS

The analysis is based on hybrid data collected by the Coihueco and HEAT telescopes and the 750 m SD array between 1 June 2010 and 31 December 2015. Subsequent data will be used in a follow-up paper. In the present paper, we use the same analysis techniques as in Aab et al. (2017a) to provide a rst search for photons in the energy range between 2 10^{17} eV and 10^{18} eV using data from the Pierre Auger Observatory. The follow-up paper will not only make use of a larger dataset, but also pro t from an analysis that is tailor-made for the low-energy enhancements of the Observatory.

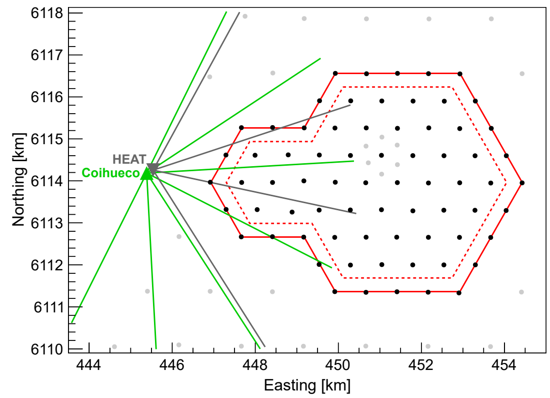

Schematic depiction of the part of the detector layout of the Pierre Auger Observatory (Aab et al. 2015a) that is relevant for the analysis discussed here. Detector stations from the 750 m SD array are shown as black points. Detector stations that are not used in this analysis (for example from the 1500 m SD array) are greyed out. The projections of the elds-of-view of the uorescence telescopes from Coihueco and HEAT on the ground are indicated by the green and gray lines, respectively. Note that Coihueco and HEAT cover di erent elevation ranges. The outline of the 750 m SD array is given by the solid red line, while the dashed red line marks the region where the shower core of an air shower event has to be located for the event to be accepted in this analysis (see Sec. 3).

Several selection criteria are applied to this dataset to ensure a good reconstruction of the air-shower events and a reliable measurement of the observables used to discriminate photon- and hadron-induced air showers (see Sec. 4). These criteria are summarized in the following.

The total dataset contains 587 475 HeCo events at the detector level, before any further selection criteria are applied. A sub-sample consisting of about 5 % of the total dataset (29 531 events, selected from the full data period using the simple prescription $_{\rm GPS}$ mod 20 = 0, where $_{\rm GPS}$ denotes the time the event was recorded in units of GPS seconds) was used as a burnt sample to optimize the event selection and perform cross-checks on the analysis. The events from the burnt sample are not used in the nal analysis.

At the geometry level of the event selection, it is required that the events are reconstructed using the hybrid event reconstruction procedure, taking into account the timing information from a triggered SD station from the 750 m SD array in addition to the FD measurements. To exclude events pointing directly towards the FD telescope, where Cherenkov light will distort the FD measurement, a minimum viewing angle of 15 is required. Lastly, only events where the shower core is reconstructed within the inner region of the 750 m SD array (marked by the dashed red line in Fig. 1) and where the zenith angle is below 60° are considered. More inclined events are not taken into account because of the absorption of the electromagnetic component of the air showers in the atmosphere and the resulting smaller trigger efficiency at lower energies.

At the third level of the event selection, the profile level, events with an unreliable reconstruction of the longitudinal profile of the air shower are discarded using a cut based on the reduced χ^2 of the fit of a Gaisser-Hillas function to the recorded profile. Events are only accepted when the reconstructed atmospheric depth of the shower maximum $X_{\max}$ is inside the geometrical field of view of the fluorescence telescopes and gaps in the recorded tracks, which can appear, for example, for air showers crossing several telescopes, amount to less than 30 % of the total observed track length. Finally, it is required that the uncertainty on the reconstructed photon energy E_γ, defined as the calorimetric energy taken from the integration of the profile plus a missing-energy correction of 1 % appropriate for primary photons (Aab et al. 2017a), is less than 20 %.

Since the precise knowledge of the atmospheric conditions is crucial for the hybrid reconstruction, events recorded during periods without information on the aerosol content of the atmosphere are not taken into account. To exclude events where the recorded profile may be distorted due to clouds over the Observatory, only events from known cloud-free periods are accepted. Events where no information on the cloud coverage is available from either the Lidar system installed at the FD site Coihueco (BenZvi et al. 2007) or infrared data from the GOES-12 satellite (Abreu et al. 2013) are excluded.

Finally, the last selection criterion removes events where fewer than four of the six SD stations in the first 750 m hexagon around the station with the largest signal are active. Such cases can occur, e.g., in the border region of the array or when individual SD stations are temporarily offline and not taking data. In this case, the discriminating observables S_b and N_{stations} (see Sec. 4) can be underestimated, mimicking air showers initiated by photons.

The numbers of events after each level of the event selection and the associated selection efficiencies are given in Tab. 1, excluding the "burnt sample" as mentioned before. The largest reduction occurs already at the geometry level. Here, the main contribution comes from the restriction of the acceptance to the area of the 750 m SD array, followed by the requirement that the events

Table 1. Numbers of events from the data sample (excluding the "burnt sample") passing the different event selection levels and the associated selection efficiencies relative to the preceding level. See the text for explanations.

Total number of HeCo events:	557 944	
After geometry level:	20 545	3.7 %
After profile level:	12 129	59.0 %
After atmosphere level:	4 373	36.1 %
After level:	3 873	88.6 %
$E_\gamma \geq 2 \times 10^{17}$ eV:	2 204	56.9 %

have to be reconstructed using the hybrid procedure. After all cuts, 2 204 events remain with a photon energy E_γ above 2×10^{17} eV.

A large sample of simulated events has been used to study the photon/hadron separation by the observables used in this analysis, to train the multivariate analysis, and to evaluate its performance. Air-shower simulations have been performed with CORSIKA (Heck et al. 1998), using EPOS LHC (Pierog et al. 2015) as the hadronic interaction model. About 72 000 photon-induced and 42 000 proton-induced air showers in six bins of equal width in $\log_{10}(E$ [eV]) between $10^{16.5}$ eV and $10^{19.5}$ eV, following a power-law spectrum with spectral index $\gamma \approx -1$ within each bin, have been used. Zenith and azimuth angles of the simulated events were drawn from an isotropic distribution between 0 and 65° and from a uniform distribution between 0 and 360°, respectively. Although they do not have a significant impact on the development of photon-induced air showers at the target energy range below 10^{18} eV, pre-showering (Erber 1966; McBreen & Lambert 1981; Homola et al. 2007) and LPM effects (Landau & Pomeranchuk 1953; Migdal 1956) were included in the simulations. Only proton-induced air showers are used as background, as these are the most "photon-like" compared to air showers induced by heavier nuclei such as helium. Even though there are indications that the composition of UHECRs is getting heavier with energy (see, e.g., Yushkov & Pierre Auger Collaboration (2019)), the assumption of a pure-proton background in the context of a search for UHE photons can be taken as a conservative "worst-case" assumption, since including heavier nuclei would always lead to a smaller estimate for the contamination in the final sample of photon candidate events.

All simulated air-shower events are processed with the Auger Offline Software Framework (Argiro et al. 2007) for a detailed simulation of the detector response. In these simulations, the actual detector status of both the SD and the FD as well as the atmospheric conditions at any given time during the aforementioned data period are taken into account, leading to a realistic estimate of the detector response. Each simulated air shower is used five times, each time with a different impact point on the ground, randomly taken from a uniform distribution encompassing the region of the 750 m SD array, and with a different event time, which was randomly determined according to the on-time of the Coihueco and HEAT telescopes during the data period used in this analysis. All simulated events are finally passed through the same event selection as the events from the data sample. After the event selection stage, the simulated samples contain about 55 000 photon-induced events and about 35 000 proton-induced events.

4. ANALYSIS

The search for primary photons presented in this work exploits the well-known differences in air-shower development for photon-induced and hadron-induced air showers: on the one hand, air showers initiated by photons develop deeper in the atmosphere than those initiated by hadrons, and on the other hand, they exhibit a smaller number of muons at ground level (Risse & Homola 2007). The first difference can be quantified through X_{max}, which can be directly measured with the FD. To complement the FD-observable X_{max}, we use another quantity determined from the data of the 750 m SD array, called S_b, which is defined as follows (Ros et al. 2011):

$$S_b = \sum_i S_i \left(\frac{r_i}{1000\,\mathrm{m}}\right)^b \quad (1)$$

where S_i denotes the measured signal in the i-th SD station at a perpendicular distance r_i to the shower axis. The parameter b has been chosen here as $b = 4$ to optimize the photon-hadron separation in accordance with Aab et al. (2017a). By construction, S_b is sensitive to the lateral distribution, which in turn depends on the depth of the air-shower development in the atmosphere and the number of muons. Hence, S_b can be used to distinguish photon- and hadron-induced air showers. In addition to X_{max} and S_b, the number of triggered SD stations $N_{stations}$ is also used in the analysis, as it has been shown in Aab et al. (2017a) that it can significantly improve the overall performance of the analysis. The distributions of X_{max}, S_b and $N_{stations}$ are shown in Fig. 2 for the simulated samples as well as the data sample.

To combine the three discriminating observables, a multivariate analysis (MVA) is performed using the Boosted Decision Tree (BDT) method as implemented by the TMVA package (Hoecker et al. 2007). To take into account energy and zenith angle dependencies, the photon energy E_0 and the zenith angle θ are also included in the MVA. The MVA is trained using two thirds of the simulated samples described before, while the remaining third is used to test the trained MVA for consistency and calculate the performance of the MVA with regard to photon/hadron separation. In Fig. 2, the training and test sub-samples are denoted by the markers and the shaded regions, respectively, for both the photon and the proton samples. In the training and testing stages of the MVA, events are weighted according to a power-law spectrum $E^{-\Gamma}$ with a spectral index $\Gamma = 2$, as in previous photon searches (see, e.g., Aab et al. (2017a)).

The distribution of the output from the BDT β, which is used as the final discriminator for separating photon-induced air showers from the hadronic background, is shown in Fig. 3 for both the simulated and the data samples (see also Sec. 5). The photon and proton distributions are clearly separated. The background rejection at a signal efficiency of 50 %, i.e., the fraction of proton-induced events that have a β larger than the median of the photon (test sample) distribution β_{cut} which is used as the photon candidate cut, marked with the dashed line in Fig. 3) is (99.87 ± 0.03) %, where the uncertainty has been determined through a bootstrapping method. When only events with $E_\gamma \geq 2 \times 10^{17}$ eV are taken into account, the background rejection at 50 % signal efficiency becomes (99.91 ± 0.03) %, hence we expect a background contamination of (0.09 ± 0.03) %. For the size of the data sample given in Tab. 1 (2 204 events), this would translate, under the assumption of a pure-proton background, to 1.98 ± 0.66 background events that are wrongly identified as photon candidate events. All of these numbers have been determined from the test samples (see above). Were the analysis to be based on X_{max} only, the background rejection at 50 % signal efficiency would be 92.5 %. The expected background contamination can therefore be reduced significantly by including the SD-related observables S_b and $N_{stations}$.

5. RESULTS

Finally, we apply the analysis to the data sample to search for the presence of photon candidate events. The distributions of the three discriminating observables X_{max}, S_b and $N_{stations}$ for the data sample are shown in Fig. 2 together with the corresponding distributions for the simulated samples. In the following paragraphs, we briefly discuss these distributions.

The X_{max} distribution for the data sample is shifted towards smaller X_{max} values compared to the proton distribution. This is in line with current Auger re-

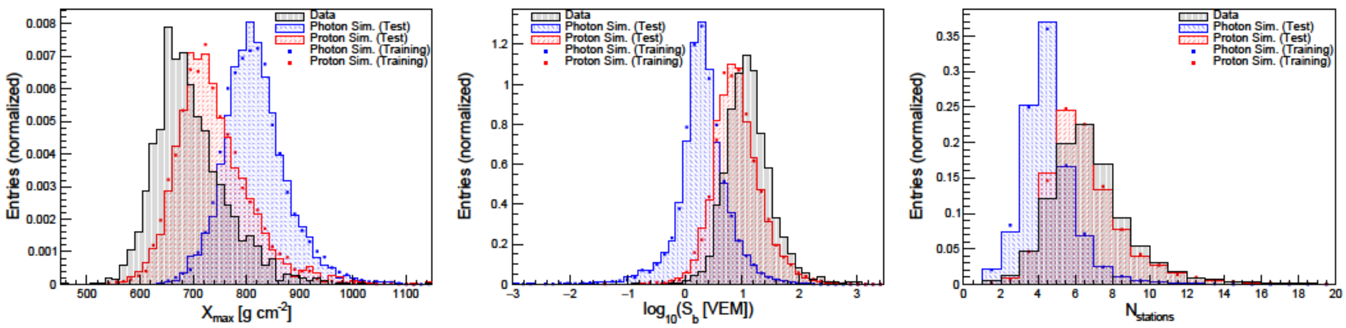

(a) (b) (c)

Figure 2. Normalized distributions of the three discriminating observables $X_{\rm max}$, S_b and $N_{\rm stations}$. The photon sample is shown in blue, the proton sample in red, and the data sample in black. Only events with $E_\gamma > 2 \times 10^{17}$ eV are shown. The simulated samples are subdivided into a training sample used to train the MVA and a test sample used to determine the separation power of the individual observables. Note that for illustrative purposes and to facilitate the comparison of the data distributions to the ones obtained from the simulated samples, the latter were weighted with an E_γ^{-3} spectrum instead of the E_γ^{-2} one used in the MVA (see Sec. 4).

sults on the composition of ultra-high-energy cosmic rays: for example, in Yushkov & Pierre Auger Collaboration (2019), the $\langle X_{\rm max} \rangle$ values that were measured above $10^{17.2}$ eV are consistently below the expectation for primary protons, indicating a heavier composition. As the average $X_{\rm max}$ is decreasing with increasing primary mass, a shift of the $X_{\rm max}$ distribution for the data sample towards smaller values is expected. Similarly, a composition effect can be seen in the S_b and $N_{\rm stations}$ distributions. As the lateral shower profile gets wider with increasing primary mass and the number of muons at ground level increases, more triggered SD stations are expected, on average, compared to primary protons (and, consequently, primary photons), leading to higher values of $N_{\rm stations}$, as well as a higher signal in these stations, which together with the higher multiplicity leads to larger S_b values. Also the choice of the hadronic interaction model—here EPOS LHC—has an impact on the distributions obtained for the simulated samples, in particular the proton distributions. Furthermore, Aab et al. (2015b, 2016a) indicate a possible underestimation of the number of muons in simulations, which can also influence the distributions.

In the next step, the MVA is applied to the 2,204 events from the data sample. The distribution of β obtained for the data sample is shown in Fig. 3 and compared to the distributions for the simulated samples. As expected from the distributions of the individual observables, on average smaller, i.e., less photon-like, values of β for the data sample than for the proton sample are found.

Finally, we use the distribution of β for the data sample to identify photon candidate events. As in Aab et al. (2017a), we use a photon candidate cut fixed to the median of the photon (test sample) distribution in the energy range $E_\gamma > 2 \times 10^{17}$ eV, which is shown in Fig. 3 as a dashed line. Zero events from the data sample have β value above the candidate cut value, hence no photon candidate events are identified. When looking at the events closest to the candidate cut, it can be noticed that their S_b values are located towards the "photon-like" tail of the distribution for primary protons at the respective energies, typically at 1.5 to 2 standard deviations from the corresponding mean values for protons. Their $X_{\rm max}$ values, however, are usually within one standard deviation from the corresponding average

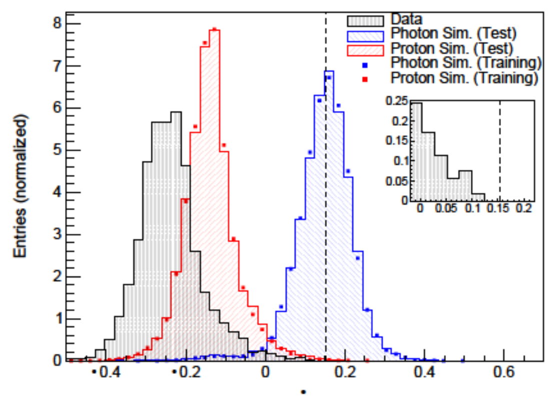

Figure 3. Normalized distributions of the final discriminator β. The photon sample is shown in blue, the proton sample in red, and the data sample in black. Only events with $E_\gamma > 2 \times 10^{17}$ eV are shown. The simulated samples are subdivided into a training sample used to train the MVA and a test sample used to determine the separation power of the full analysis. The dashed line denotes the median of the photon test sample, which is used as the photon candidate cut. The inlay shows a zoom on the data distribution around the photon candidate cut.

for protons. Regarding N_{stations}, a similar behaviour as for S_b is found. In the combination of the individual observables in the MVA, the resulting value of β is below the photon candidate cut.

We calculate the final results of this study in terms of upper limits on the integral flux of photons $\Phi^{\mathrm{C.L.}}_{\gamma,\,\mathrm{U.L.}}(E_\gamma{>}E_0)$, where C.L. denotes the confidence level at which we determine the upper limits. $\Phi^{\mathrm{C.L.}}_{\gamma,\,\mathrm{U.L.}}(E_\gamma{>}E_0)$ is calculated according to

$$\Phi^{\mathrm{C.L.}}_{\gamma,\,\mathrm{U.L.}}(E_\gamma{>}E_0) = \frac{N_\gamma^{\mathrm{C.L.}}}{\epsilon_{\mathrm{cand}}\times(1-f_{\mathrm{burnt}})\times\mathcal{E}_\gamma}, \quad (2)$$

where $N_\gamma^{\mathrm{C.L.}}$ is the upper limit on the number of photon candidate events at the given confidence level calculated using the Feldman-Cousins approach (Feldman & Cousins 1998) with no background subtraction, ϵ_{cand} is the efficiency of the photon candidate cut, f_{burnt} is the fraction of the data used as a "burnt sample", and $\mathcal{E}_\gamma$ is the integrated efficiency-weighted exposure for photons (see also Tab. 2). $\mathcal{E}_\gamma$ is calculated from simulations as

$$\mathcal{E}_\gamma(E_\gamma{>}E_0) = \int_{E_0}^{\infty} \frac{E_\gamma^{-\Gamma}}{c_E}\,\epsilon_\gamma(E_\gamma,t,\theta,\varphi,x,y)\,\mathrm{d}S\,\mathrm{d}t\,\mathrm{d}\Omega\,\mathrm{d}E_\gamma, \quad (3)$$

where $\epsilon_\gamma(E_\gamma,t,\theta,\varphi,x,y)$ is the overall efficiency for photons—excluding the final photon candidate cut—depending on the photon energy E_γ, the time t, the zenith angle θ, the azimuth angle φ and the coordinates x and y of the impact point of the air shower on the ground. The integration is performed over the area S, the time t, the solid angle Ω, and the photon energy E_γ. The normalization factor c_E is calculated through

$$c_E = \int_{E_0}^{\infty} E_\gamma^{-\Gamma}\,\mathrm{d}E_\gamma. \quad (4)$$

The result of the integration following Eq. 3 with a spectral index $\Gamma = 2$ is shown in Fig. 4. In the energy range of interest between $2{\times}10^{17}$ eV and 10^{18} eV, the weighted exposure varies between 2.4 and 2.7 km^2 yr sr, with a maximum at $3.5{\times}10^{17}$ eV. Towards lower energies, the exposure becomes smaller because lower-energy air showers trigger the detector with reduced efficiency. Towards higher energies, the dominant cause for the decrease in exposure is the event selection, because showers where X_{max} is reconstructed to be below the field of view of the telescopes are excluded from the analysis (see Sec. 3).

We place upper limits on the integral photon flux $\Phi^{\mathrm{C.L.}}_{\gamma,\,\mathrm{U.L.}}(E_\gamma{>}E_0)$ at threshold energies of 2, 3, and $5{\times}10^{17}$ eV, as well as 10^{18} eV, at a confidence level of 95 %. At these threshold energies, the upper limits are 2.72, 2.50, 2.74, and 3.55 km^{-2} yr^{-1} sr^{-1}, respectively.

The quantities needed to calculate the upper limits according to Eq. 2 are listed in Tab. 2. For completeness, we also calculated upper limits at a confidence level of 90 %, as used e.g. in Apel et al. (2017) and Fomin et al. (2017). The upper limits in this case are 2.15, 1.97, 2.16, and 2.79 km^{-2} yr^{-1} sr^{-1} at the same threshold energies. Using the energy spectrum of cosmic rays measured by the Pierre Auger Observatory (Abreu et al. 2021), the upper limits on the integral photon flux can be translated into upper limits on the integral photon fraction. At a confidence level of 95 %, these are 0.28 %, 0.63 %, 2.20 % and 13.8 % for the same threshold energies as above.

To assess the impact on the final results of the choice of hadronic interaction models and of the assumptions on the composition of primary cosmic rays, smaller samples of proton-induced air showers simulated with the hadronic interaction models QGSJET-II-04 (Ostapchenko 2011) and SIBYLL 2.3c (Fedynitch et al. 2019) and of air showers induced by iron nuclei, simulated with EPOS LHC, have been used. Each of these samples contains 30,000 air-shower events. The analysis has been repeated replacing the default background sample (primary protons simulated with EPOS LHC) by primary protons simulated with QGSJET-II-04 and SIBYLL 2.3c and with a mixture of 50 % primary protons and 50 % primary iron nuclei (both simulated with EPOS LHC). In all cases, no photon candidate events were identified in the data sample, indicating that the analysis is robust against these assumptions. Likewise, varying the spectral index Γ from 2 to, e.g., 1.5 or 2.5, and repeating the analysis does not change the observed number of photon candidates (0). It should be

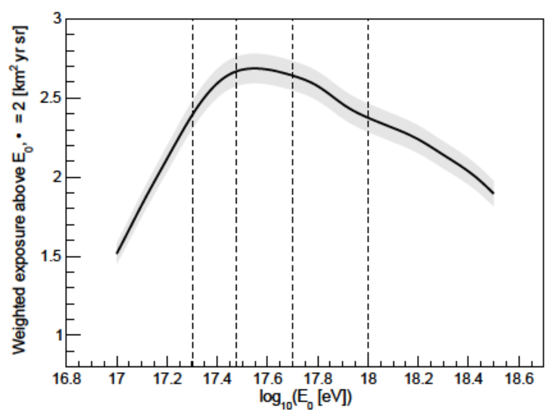

Figure 4. Integrated efficiency-weighted hybrid exposure for photons, calculated from simulations following Eq. 3 under the assumption $\Gamma = 2$, with the statistical uncertainties shown as a grey band. The dashed lines denote the energy thresholds at which upper limits on the integral photon flux are placed in this analysis.

Upper limits on the integral photon ux, determined at 95 % C.L., calculated using Eq. 2. See the text for explanations.

[eV]					1	$\mathcal{E}$ [km yr sr]	[km^{-} yr^{-} sr^{-}]
2 10	2,204	0	3.095	0.50	0.96	2.38	2.72
3 10	1,112	0	3.095	0.48	0.96	2.69	2.50
5 10	333	0	3.095	0.45	0.94	2.68	2.74
10	67	0	3.095	0.38	0.94	2.41	3.55

taken into account however, that also enters the calculation of the weighted exposure, leading to a change in the nal upper limits by, on average, 5 %. Finally, we studied the impact of possible systematic uncertainties in the measurement of the observables. Changing the $_{max}$ values of all events in the data sample by 10 g cm ^{2} (Bellido & Pierre Auger Collaboration 2017) does not change the number of photon candidate events. Likewise, changing the values of all events in the data sample by 5 % (Aab et al. 2017a) has no e ect on the number of photon candidate events. These tests show that the analysis is also robust against systematic uncertainties in the measured observables.

6. DISCUSSION AND CONCLUSIONS

The upper limits on the integral photon ux derived in the previous section are shown in Fig. 5, together with the results of other photon searches with energy thresholds ranging from 10^{16} eV to 10^{20} eV. In the energy region below 10^{18} eV, the limits obtained in this study are the most stringent ones, improving previous limits from KASCADE-Grande (Apel et al. 2017) and EAS-MSU (Fomin et al. 2017) by up to an order of magnitude. The analysis presented here extends the energy range of photon searches at the Pierre Auger Observatory and complements previous analyses in the energy range above 10^{19} eV (Rautenberg & Pierre Auger Collaboration 2019) and between 10^{18} eV and 10^{19} eV (Savina & Pierre Auger Collaboration 2021), closing the gap to the smaller air-shower experiments mentioned before. For a threshold energy of 10^{18} eV, the upper limit determined in this analysis is about two orders of magnitude above the previous limit from Savina & Pierre Auger Collaboration (2021), which is due mainly to the smaller exposure, which in turn is a consequence of the smaller size of the 750 m SD array compared to the full array. Overall, the Pierre Auger Observatory now provides the most stringent limits on the incoming UHE photon ux over three decades in energy. This set of upper limits allows us to draw some conclusions relevant to the astrophysics of UHECRs and beyond, which we now discuss.

A guaranteed ux of ultra-high-energy photons of cosmogenic origin is that resulting from interactions of UHECRs with the background photon elds permeating the Universe, most notably the cosmic microwave background (Greisen 1966; Zatsepin & Kuzmin 1966). This ux is much reduced relative to that of UHECRs due to, as pointed out in the introduction, the short photon horizon (a few hundred kpc) compared to the cosmic-ray one (from a few tens of Mpc above the GZK threshold to cosmological scales below). Although guaranteed, the precise knowledge of this ux su ers from several uncertainties. The production channel of these photons is the decay of ^{0} mesons. The hadrons that cause the creation of these mesons may be primary proton cosmic rays, or secondary ones mainly produced by the photo-disintegration of nuclei interacting inelastically with a cosmic background photon. Since the nucleons produced in a photo-disintegration reaction inherit the energy of the fragmented nucleus divided by its atomic number, the photons ultimately produced from primary heavy nuclei are of lower energies than those from lighter ones or from proton primaries. The photon ux, therefore, depends on the nature of the UHECRs, which remains poorly constrained above about 5 10^{19} eV. The expectation for a pure-proton scenario is shown as the red band in Fig. 5 (Kampert et al. 2011), while that for a mixed composition at the sources is shown as the green band (Bobrikova et al. 2021). The latter, which is an order of magnitude lower than the former and falls o much faster, is in agreement with the various constraints inferred from the data collected at the Observatory, namely the mass composition and the energy spectrum (Aab et al. 2017b). Other dependencies that explain the width of the bands come from the hypotheses on the maximum acceleration energy of the nuclei at the sources and on the shape of the energy spectrum of the accelerated particles. Overall, while the sensitivities reached above about 3 10^{18} eV approach the most optimistic expectations of the cosmogenic photon ux from protons, they are about 1 5 orders of magnitude above those from the mixed-composition model.

Another cosmogenic ux is that from the interactions of UHECRs with the matter traversed in the Galactic plane, which is larger than the aforementioned one below about 10^{18} eV (Berat et al. 2022). Shown in blue, the width of the band accounts for uncertainties arising from the distribution of the gas in the disk, the absolute level

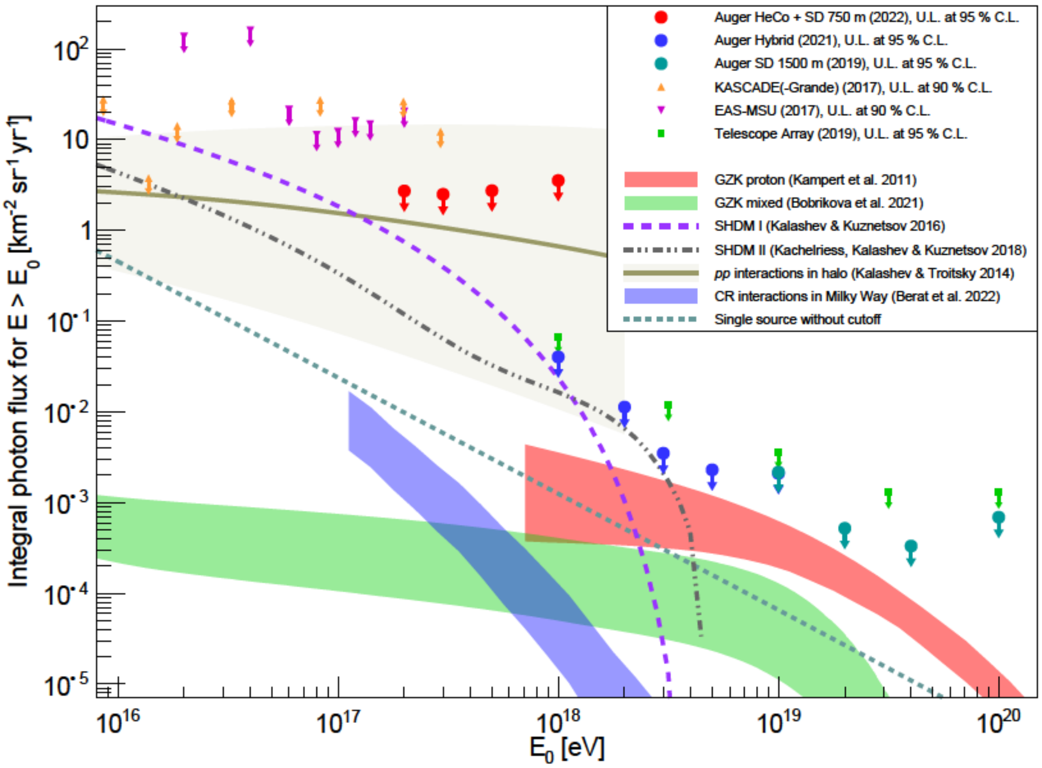

Figure 5. Upper limits (at 95 % C.L.) on the integral photon flux above 2×10^{17} eV determined here (red circles). Shown are also previous upper limits by various experiments: Pierre Auger Observatory (hybrid: blue circles, taken from Savina & Pierre Auger Collaboration (2021); SD: cyan circles, taken from Rautenberg & Pierre Auger Collaboration (2019)), KASCADE/KASCADE-Grande (orange triangles, taken from Apel et al. (2017)), EAS-MSU (magenta diamonds, taken from Fomin et al. (2017)) and Telescope Array (green squares, taken from Abbasi et al. (2019)). The red band denotes the range of expected GZK photon fluxes under the assumption of a pure-proton scenario (Kampert et al. 2011). The green band shows the expected GZK photon flux assuming a mixed composition that would fit the Auger data (Bobrikova et al. 2021). In addition, the expected photon fluxes from the decay of super-heavy dark matter particles are included (decay into hadrons: dashed violet line, based on Kalashev & Kuznetsov (2016); decay into leptons: dot-dashed gray line, based on Kachelriess et al. (2018); the exact lines have been obtained through personal communication with one of the authors). The photon fluxes that would be expected from *pp* interactions in the Galactic halo (Kalashev & Troitsky (2014), olive-green line) or from cosmic-ray interactions with matter in the Milky Way (Bérat et al. (2022), blue band) are shown as well. Also included is the expected flux of photons from a single, putative source without a cutoff in its spectrum (dotted turquoise line, modeled after HAWC J1825-134, Albert et al. (2021), where we extrapolated the measured flux to the highest energies), ignoring its directionality as if its flux were distributed over the full sky.

of the UHECR flux, and the mass composition. The limits obtained in this study improve previous ones in the energy range of interest to probe such a flux; yet they remain between two and three orders of magnitude above the expectations.

The cosmogenic fluxes just mentioned can be seen as floors above which increased sensitivity to photons could reveal unexpected phenomena. To exemplify such a potential, we explain below the four curves that correspond to fluxes from putative sources in the Galactic disk or to patterns that could emerge from proton-proton interactions in the halo of the Galaxy or from the decay of super-heavy dark matter (SHDM).

The recent observation of photons above 2×10^{14} eV from decaying neutral pions from the J1825-134 source reported in Albert et al. (2021), in a direction coincident with a giant molecular cloud, provides evidence that cosmic rays are indeed accelerated to energies of several 10^{15} eV, and above, in the Galaxy. Interestingly, the flux of this source could extend well beyond 2×10^{14} eV, as no cutoff is currently observed in its energy spectrum measured up to this energy. As an example of the discovery potential with increased exposure, we show as the green curve the flux from such a putative source extrapolated to the highest energies. Note that this flux, which is directional in essence, is here for simplicity calculated by converting it to a diffuse one, assuming the flux were distributed over the full sky. We observe that the extrapolated flux for this source is higher than the cosmogenic ones below 10^{18} eV. The upper limits determined here exceed the extrapolated flux of this single, specific source by two orders of magnitude. They nevertheless limit the effective number of similar sources in the Galaxy. Improved tests of the abundance of such putative sources will be possible by further increasing the sensitivity of photon searches in this energy region or decreasing the energy threshold.

The origin of the bulk of the high-energy neutrino flux observed at the IceCube observatory (see, e.g., Aartsen et al. (2020)) is still debated. However, their production mechanism is conventionally considered as that of high-energy hadronic or photo-hadronic interactions that create charged pions decaying into neutrinos. These same interactions produce neutral pions that decay into photons. Therefore, there is an expected connection between high-energy photons and high-energy neutrinos. Since the horizon of photons is much smaller than that of neutrinos, they can trace the local sources in a way that could facilitate the differentiation between different scenarios. In Fig. 5, we reproduce in olive green the expectations for cosmic-ray interactions with the hot gas filling the outer halo of the Galaxy up to hundreds of kiloparsecs, as estimated in Kalashev & Troitsky (2014) by requiring that this photon flux is the counterpart of the neutrino one. The width of the band reflects the uncertainties in the spectral shape of the neutrino flux. We observe that the limits derived in this study are already constraining.

Finally, UHE photons could also result from the decay of SHDM particles. We note that previous upper limits on the incoming photon flux already severely constrained non-acceleration models in general, and SHDM models in particular, trying to explain the origin of cosmic rays at the highest energies (see, e.g., Abraham et al. (2008); Aab et al. (2017a)). Still, the production of super-heavy particles in the early Universe remains a possible solution to the dark matter conundrum because of the high value of the instability energy scale in the Standard Model of particle physics, which, according to current measurements of the Higgs-boson mass and the Yukawa coupling of the top quark, ranges between 10^{10} and 10^{12} GeV (Degrassi et al. 2012; Bednyakov et al. 2015). The Standard Model can, therefore, be extrapolated without encountering inconsistencies that would make the electroweak vacuum unstable up to such energy scales (and even to much higher ones given the slow evolution of the instability scale up to the Planck mass (Degrassi et al. 2012)), where new physics could arise, giving rise to a mass spectrum of super-heavy particles that could have been produced during post-inflation reheating by various mechanisms (see, e.g., Ellis et al. (1992); Berezinsky et al. (1997); Chung et al. (1998); Garny et al. (2016); Ellis et al. (2016); Dudas et al. (2017); Kaneta et al. (2019); Mambrini & Olive (2021)). The set of limits shown in Fig. 5 allows for constraining the phase space of mass and lifetime of the SDHM particles (see, e.g., Kalashev & Kuznetsov (2016); Kachelriess et al. (2018); Berat et al. (2022)). To illustrate the discovery potential with searches for UHE photons, we show as the dashed violet line and the dot-dashed gray line the expected photon fluxes in the case of hadronic (Kalashev & Kuznetsov 2016) and leptonic (Kachelriess et al. 2018) decay channels, respectively. For these lines, we assume that the mass of the SHDM particles is 10^{10} GeV and their lifetime is 3×10^{21} yr, as currently allowed by previous limits. As the sensitivity of current photon searches increases, it will be possible to further constrain these values (Anchordoqui et al. 2021).

Further improvements of the upper limits derived in this analysis can be expected not only from using a larger dataset, profiting from the constant increase in exposure over time, but also from the ongoing detector upgrade of the Pierre Auger Observatory, dubbed AugerPrime (Castellina & Pierre Auger Collaboration 2019; Aab et al. 2016b). A major part of this upgrade is the installation of scintillation detectors on top of the water-Cherenkov detector stations of the SD, with the aim to better separate the muonic and electromagnetic components of an air shower. Current photon searches already exploit the differences in these components between photon- and hadron-induced air showers, albeit in a rather indirect way. AugerPrime will allow for a more direct access, which will lead to an overall better separation between photon-induced air showers and the vast hadronic background. Naturally, this upgrade will improve the upper limits on the incoming photon flux or, in the best case, lead to the unambiguous detection of photons at ultra-high energies.

ACKNOWLEDGMENTS

The successful installation, commissioning, and operation of the Pierre Auger Observatory would not have been possible without the strong commitment and effort from the technical and administrative staff in Malargue. We are very grateful to the following agencies and organizations for financial support:

Argentina – Comision Nacional de Energía Atomica; Agencia Nacional de Promocion Científica y Tecnologica (ANPCyT); Consejo Nacional de Investigaciones Científicas y Tecnicas (CONICET); Gobierno de la Provincia de Mendoza; Municipalidad de Malargue; NDM Holdings and Valle Las Lenas; in gratitude for their continuing cooperation over land access; Australia the Australian Research Council; Belgium Fonds de la Recherche Scienti que (FNRS); Research Foundation Flanders (FWO); Brazil Conselho Nacional de Desenvolvimento Cient co e Tecnologico (CNPq); Financiadora de Estudos e Projetos (FINEP); Fundacao de Amparo a Pesquisa do Estado de Rio de Janeiro (FAPERJ); Sao Paulo Research Foundation (FAPESP) Grants No. 2019/10151-2, No. 2010/07359-6 and No. 1999/05404-3; Ministerio da Ciencia, Tecnologia, Inovacoes e Comunicacoes (MCTIC); Czech Republic Grant No. MSMT CR LTT18004, LM2015038, LM2018102, CZ.02.1.01/0.0/0.0/16_013/0001402, CZ.02.1.01/0.0/0.0/18_046/0016010 and CZ.02.1.01/0.0/0.0/17_049/0008422; France Centre de Calcul IN2P3/CNRS; Centre National de la Recherche Scienti que (CNRS); Conseil Regional Ile-de-France; Departement Physique Nucleaire et Corpusculaire (PNC-IN2P3/CNRS); Departement Sciences de l Univers (SDU-INSU/CNRS); Institut Lagrange de Paris (ILP) Grant No. LABEX ANR-10-LABX-63 within the Investissements d Avenir Programme Grant No. ANR-11-IDEX-0004-02; Germany Bundesministerium fur Bildung und Forschung (BMBF); Deutsche Forschungsgemeinschaft (DFG); Finanzministerium Baden-Wurttemberg; Helmholtz Alliance for Astroparticle Physics (HAP); Helmholtz-Gemeinschaft Deutscher Forschungszentren (HGF); Ministerium fur Innovation, Wissenschaft und Forschung des Landes Nordrhein-Westfalen; Ministerium fur Wissenschaft, Forschung und Kunst des Landes Baden-Wurttemberg; Italy Istituto Nazionale di Fisica Nucleare (INFN); Istituto Nazionale di Astro sica (INAF); Ministero dell Istruzione, dell Universita e della Ricerca (MIUR); CETEMPS Center of Excellence; Ministero degli A ari Esteri (MAE); Mexico Consejo Nacional de Ciencia y Tecnolog a (CONACYT) No. 167733; Universidad Nacional Autonoma de Mexico (UNAM); PAPIIT DGAPA-UNAM; The Netherlands Ministry of Education, Culture and Science; Netherlands Organisation for Scienti c Research (NWO); Dutch national e-infrastructure with the support of SURF Cooperative; Poland Ministry of Education and Science, grant No. DIR/WK/2018/11; National Science Centre, Grants No. 2016/22/M/ST9/00198, 2016/23/B/ST9/01635, and 2020/39/B/ST9/01398; Portugal Portuguese national funds and FEDER funds within Programa Operacional Factores de Competitividade through Fundacao para a Ciencia e a Tecnologia (COMPETE); Romania Ministry of Research, Innovation and Digitization, CNCS/CCCDI UEFISCDI, projects PN19150201/16N/2019, PN1906010, TE128 and PED289, within PNCDI III; Slovenia Slovenian Research Agency, grants P1-0031, P1-0385, I0-0033, N1-0111; Spain Ministerio de Econom a, Industria y Competitividad (FPA2017-85114-P and PID2019-104676GB-C32), Xunta de Galicia (ED431C 2017/07), Junta de Andaluc a (SOMM17/6104/UGR, P18-FR-4314) Feder Funds, RENATA Red Nacional Tematica de Astropart culas (FPA2015-68783-REDT) and Mar a de Maeztu Unit of Excellence (MDM-2016-0692); USA Department of Energy, Contracts No. DE-AC02-07CH11359, No. DE-FR02-04ER41300, No. DE-FG02-99ER41107 and No. DE-SC0011689; National Science Foundation, Grant No. 0450696; The Grainger Foundation; Marie Curie-IRSES/EPLANET; European Particle Physics Latin American Network; and UNESCO.

REFERENCES

Aab, A., et al. 2015a, Nucl. Instrum. Meth. A, 798, 172, doi: 10.1016/j.nima.2015.06.058

. 2015b, Phys. Rev. D, 91, 032003, doi: 10.1103/PhysRevD.91.032003

. 2016a, Phys. Rev. Lett., 117, 192001, doi: 10.1103/PhysRevLett.117.192001

. 2016b. https://arxiv.org/abs/1604.03637

. 2017a, J. Cosmol. Astropart. Phys., 04, 009, doi: 10.1088/1475-7516/2017/04/009

. 2017b, J. Cosmol. Astropart. Phys., 04, 038, doi: 10.1088/1475-7516/2017/04/038

Aartsen, M. G., et al. 2020, Phys. Rev. Lett., 125, 121104, doi: 10.1103/PhysRevLett.125.121104

Abbasi, R. U., et al. 2019, Astropart. Phys., 110, 8, doi: 10.1016/j.astropartphys.2019.03.003

Abraham, J., et al. 2008, Astropart. Phys., 29, 243, doi: 10.1016/j.astropartphys.2008.01.003

Abreu, P., et al. 2013, Astropart. Phys., 50-52, 92, doi: 10.1016/j.astropartphys.2013.09.004

. 2021, Eur. Phys. J. C, 81, 966, doi: 10.1140/epjc/s10052-021-09700-w

Albert, A., et al. 2021, Astrophys. J. Lett., 907, L30, doi: 10.3847/2041-8213/abd77b

Alcantara, E., Anchordoqui, L. A., & Soriano, J. F. 2019, Phys. Rev. D, 99, 103016, doi: 10.1103/PhysRevD.99.103016

Aloisio, R., Berezinsky, V., & Kachelriess, M. 2006, Phys. Rev. D, 74, 023516, doi: 10.1103/PhysRevD.74.023516

Amenomori, M., et al. 2021, Phys. Rev. Lett., 126, 141101, doi: 10.1103/PhysRevLett.126.141101

Anchordoqui, L. A., et al. 2021, Astropart. Phys., 132, 102614, doi: 10.1016/j.astropartphys.2021.102614

Apel, W. D., et al. 2017, Astrophys. J., 848, 1, doi: 10.3847/1538-4357/aa8bb7

Argiro, S., Barroso, S. L. C., Gonzalez, J., et al. 2007, Nucl. Instrum. Meth. A, 580, 1485, doi: 10.1016/j.nima.2007.07.010

Bednyakov, A. V., Kniehl, B. A., Pikelner, A. F., & Veretin, O. L. 2015, Phys. Rev. Lett., 115, 201802, doi: 10.1103/PhysRevLett.115.201802

Bellido, J., & Pierre Auger Collaboration. 2017, Proc. 35th International Cosmic Ray Conference (Busan, Korea), PoS (ICRC2017), 506, doi: 10.22323/1.301.0506

Benson, A., Wolfendale, A. W., & Smialkowski, A. 1999, Astropart. Phys., 10, 313, doi: 10.1016/S0927-6505(98)00065-6

BenZvi, S. Y., et al. 2007, Nucl. Instrum. Meth. A, 574, 171, doi: 10.1016/j.nima.2007.01.094

Berat, C., Bleve, C., Deligny, O., et al. 2022, accepted for publication in Astrophys. J. https://arxiv.org/abs/2203.08751

Berezinsky, V., Kachelrie , M., & Vilenkin, A. 1997, Phys. Rev. Lett., 79, 4302, doi: 10.1103/PhysRevLett.79.4302

Berezinsky, V., & Mikhailov, A. A. 1999, Phys. Lett. B, 449, 237, doi: 10.1016/S0370-2693(99)00053-2

Bobrikova, A., Niechciol, M., Risse, M., & Ruehl, P. 2021, Proc. 37th International Cosmic Ray Conference (Berlin, Germany), PoS (ICRC2021), 449, doi: 10.22323/1.395.0449

Cao, Z., et al. 2021a, Nature, 594, 33 36, doi: https://doi.org/10.1038/s41586-021-03498-z

. 2021b, Astrophys. J. Lett., 919, L22. https://arxiv.org/abs/2106.09865

Castellina, A., & Pierre Auger Collaboration. 2019, EPJ Web Conf., 210, 06002, doi: 10.1051/epjconf/201921006002

Chung, D. J., Kolb, E. W., & Riotto, A. 1998, Phys. Rev. D, 59, 023501, doi: 10.1103/PhysRevD.59.023501

Degrassi, G., Di Vita, S., Elias-Miro, J., et al. 2012, J. High Energy Phys., 08, 098, doi: 10.1007/JHEP08(2012)098

Dudas, E., Mambrini, Y., & Olive, K. 2017, Phys. Rev. Lett., 119, 051801, doi: 10.1103/PhysRevLett.119.051801

Ellis, J., Garcia, M. A. G., Nanopoulos, D. V., Olive, K. A., & Peloso, M. 2016, J. Cosmol. Astropart. Phys., 03, 008, doi: 10.1088/1475-7516/2016/03/008

Ellis, J. R., Gelmini, G., Lopez, J. L., Nanopoulos, D. V., & Sarkar, S. 1992, Nucl. Phys. B, 373, 399, doi: 10.1016/0550-3213(92)90438-H

Erber, T. 1966, Rev. Mod. Phys., 38, 626, doi: 10.1103/RevModPhys.38.626

Fedynitch, A., Riehn, F., Engel, R., Gaisser, T. K., & Stanev, T. 2019, Phys. Rev. D, 100, 103018, doi: 10.1103/PhysRevD.100.103018

Feldman, G. J., & Cousins, R. D. 1998, Phys. Rev. D, 57, 3873, doi: 10.1103/PhysRevD.57.3873

Fomin, Y. A., Kalmykov, N. N., Karpikov, I. S., et al. 2017, Phys. Rev. D, 95, 123011, doi: 10.1103/PhysRevD.95.123011

Garny, M., Sandora, M., & Sloth, M. S. 2016, Phys. Rev. Lett., 116, 101302, doi: 10.1103/PhysRevLett.116.101302

Gelmini, G., Kalashev, O. E., & Semikoz, D. V. 2008, J. Exp. Theor. Phys., 106, 1061, doi: 10.1134/S106377610806006X

Greisen, K. 1966, Phys. Rev. Lett., 16, 748, doi: 10.1103/PhysRevLett.16.748

Heck, D., Knapp, J., Capdevielle, J. N., Schatz, G., & Thouw, T. 1998, FZKA-6019

Hoecker, A., et al. 2007, CERN-OPEN-2007-007. https://arxiv.org/abs/physics/0703039

Homola, P., Risse, M., Engel, R., et al. 2007, Astropart. Phys., 27, 174, doi: 10.1016/j.astropartphys.2006.10.005

Kachelriess, M., Kalashev, O. E., & Kuznetsov, M. Y. 2018, Phys. Rev. D, 98, 083016, doi: 10.1103/PhysRevD.98.083016

Kalashev, O. E., & Troitsky, S. V. 2014, Pisma Zh. Eksp. Teor. Fiz., 100, 865, doi: 10.1134/S0021364014240072

Kalashev, O. K., & Kuznetsov, M. Y. 2016, Phys. Rev. D, 94, 063535, doi: 10.1103/PhysRevD.94.063535

Kampert, K.-H., et al. 2011, Proc. 32nd International Cosmic Ray Conference (Beijing, China), doi: 10.7529/ICRC2011/V02/1087

Kaneta, K., Mambrini, Y., & Olive, K. A. 2019, Phys. Rev. D, 99, 063508, doi: 10.1103/PhysRevD.99.063508

Landau, L. D., & Pomeranchuk, I. 1953, Dokl. Akad. Nauk Ser. Fiz., 92, 535

Mambrini, Y., & Olive, K. A. 2021, Phys. Rev. D, 103, 115009, doi: 10.1103/PhysRevD.103.115009

McBreen, B., & Lambert, C. J. 1981, Phys. Rev. D, 24, 2536, doi: 10.1103/PhysRevD.24.2536

Medina-Tanco, G. A., & Watson, A. A. 1999, Astropart. Phys., 12, 25. https://arxiv.org/abs/astro-ph/9905240

Migdal, A. B. 1956, Phys. Rev., 103, 1811, doi: 10.1103/PhysRev.103.1811

Ostapchenko, S. 2011, Phys. Rev. D, 83, 014018, doi: 10.1103/PhysRevD.83.014018

Pierog, T., Karpenko, I., Katzy, J. M., Yatsenko, E., & Werner, K. 2015, Phys. Rev. C, 92, 034906, doi: 10.1103/PhysRevC.92.034906

Rautenberg, J., & Pierre Auger Collaboration. 2019, Proc. 36th International Cosmic Ray Conference (Madison, USA), PoS (ICRC2019), 398, doi: 10.22323/1.358.0398

Risse, M., & Homola, P. 2007, Mod. Phys. Lett. A, 22, 749, doi: 10.1142/S0217732307022864

Ros, G., Supanitsky, A. D., Medina-Tanco, G. A., et al. 2011, Astropart. Phys., 35, 140, doi: 10.1016/j.astropartphys.2011.06.011

Savina, P., & Pierre Auger Collaboration. 2021, Proc. 37th International Cosmic Ray Conference (Berlin, Germany), PoS (ICRC2021), 373, doi: 10.22323/1.395.0373

Si ert, B. B., Lazarotto, B., de Mello Neto, J. R. T., & Olinto, A. 2007, Braz. J. Phys., 37, 48, doi: 10.1590/S0103-97332007000100016

Yushkov, A., & Pierre Auger Collaboration. 2019, Proc. 36th International Cosmic Ray Conference (Madison, USA), PoS (ICRC2019), 482, doi: 10.22323/1.358.0482

Zatsepin, G. T., & Kuzmin, V. A. 1966, JETP Lett., 4, 78